The Cryosphere
Open Access
Discussions

The effect of snow/sea ice type on the response of albedo and light penetration depth (e-folding depth) to increasing black carbon

A. A. Marks and M. D. King

Department of Earth Sciences, Royal Holloway University of London, Egham, Surrey, TW20 0EX, UK

Correspondence to: M. D. King (m.king@es.rhul.ac.uk)

TCD

8, 1023–1056, 2014

BC in snow and sea ice

A. A. Marks and
M. D. King

Title Page

Abstract	Introduction
Conclusions	References
Tables	Figures

◄◄ ►►

◄ ►

Back Close

Full Screen / Esc

Printer-friendly Version

Interactive Discussion

BC in snow and sea ice

A. A. Marks and
M. D. King

Title Page

Abstract | Introduction

Conclusions | References

Tables | Figures

|◄ | ►|

◄ | ►

Back | Close

Full Screen / Esc

Printer-friendly Version

Interactive Discussion

Abstract

The optical properties of snow/sea ice vary with age and by the processes they were formed, giving characteristic types of snow and sea ice. The response of albedo and light penetration depth (e-folding depth) to increasing mass-ratio of black carbon is shown to depend on the snow and sea ice type and the thickness of the snow or sea ice. The response of albedo and e-folding depth of three different types of snow (cold polar snow, windpacked snow and melting snow) and three sea ice (multi-year ice, first-year ice and melting sea ice) to increasing black carbon is calculated using a coupled atmosphere–snow/sea ice radiative-transfer model (TUV-snow), over the optical wavelengths of 300–700 nm. The snow and sea ice types are defined by a scattering-cross section, density and asymmetry parameter. The relative change in albedo of a melting snowpack is a factor of four more responsive to additions of black carbon compared to cold polar snow over a black carbon increase from 1 to 50 ng g^{-1}. While the relative change in albedo of a melting sea ice is a factor of two more responsive to additions of black carbon compared to multi-year ice for the same black carbon mass-ratio increase. The response of e-folding depth is effectively not dependent on snow/sea ice type. The albedo of sea ice is more responsive to increased mass-ratios of black carbon than snow.

1   Introduction

Black carbon, a component of soot formed by incomplete combustion, strongly absorbs solar radiation (e.g. Mitchell, 1957; Highwood and Kinnersley, 2006; Hansen and Nazarenko, 2004; Jacobson, 2001; Ramanathan and Carmichael, 2008; Bond et al., 2013). Back carbon deposited onto snow and sea ice causes increased absorption of incident solar radiation, decreased surface albedo and thus exacerbated melting (e.g. Chýlek et al., 1983; Warren, 1984; Warren and Wiscombe, 1985; Clarke and Noone, 1985; Ledley and Thompson, 1986; Warren and Clarke, 1990; Light et al., 1998; Gren-

A. A. Marks and
M. D. King

Title Page

Abstract | Introduction

Conclusions | References

Tables | Figures

|◀ | ▶|

◀ | ▶

Back | Close

Full Screen / Esc

Printer-friendly Version

Interactive Discussion

fell et al., 2002; Jacobson, 2004; Flanner et al., 2007; Doherty et al., 2010; Yasunari et al., 2011; Painter et al., 2012; Reay et al., 2012; France et al., 2012; Goldenson et al., 2012; Holland et al., 2012; Bond et al., 2013). The deposition of black carbon also shortens light penetration depths or e-folding depths (the depth of snow over which

5 light intensity reduces to $\frac{1}{e}$), which can affect photochemical and photobiological processes that occur in snow/sea ice (e.g. Reay et al., 2012; France et al., 2012; Zatko et al., 2013). Black carbon accounts for 85 % of absorption by all light absorbing impurities in snow/sea ice (Bond et al., 2013), with absorption by dust also being important. There is still a large degree of uncertainty in the possible effects of black carbon in

10 snow and sea ice, for example, the 2007 IPCC report suggested the positive radiative forcing due to black carbon in snow is 0.1 W m^{-2}, with a 100 % error in this value (Solomon et al., 2007). The next IPCC report is due soon.

Snow and sea ice varies both laterally and temporally in terms of thickness, density and grain size which causes variation in the optical and physical properties of snow

15 and sea ice. Propagation of light in snow/sea ice is dependent on absorption and scattering of photons within the medium. In snow, absorption of solar radiation is due to ice and the light absorbing impurities within the snow, while in sea ice absorption is due to brine, ice and impurities. In snow and sea ice, absorption by air is considered to be negligible (Perovich, 1996). Scattering of light in snow occurs at air–ice bound-

20 aries owing to air between the ice grains. Light scattering in sea ice occurs at the ice–air boundaries of air bubbles trapped in the ice and at the ice–brine boundaries of brine/ice channel/pockets (Perovich, 1996). The dominating scattering interface depends on the prevalence of air bubbles within the ice (Perovich, 1996). Excellent reviews of the optical properties of snow and sea ice are found in Warren (1982) and

25 Perovich (1996) respectively. It is expected that different types of snow and sea ice will respond differently to additions of light absorbing impurities such as black carbon. Warren (1982) and Hadley and Kirchstetter (2012) show that for a given amount of light absorbing impurity a greater reduction in albedo for coarse-grained snow than for fine-grained snow is achieved. Using the model of Warren and Wiscombe (1980);

Warren (1982) calculated the effect of volcanic ash on the albedo of snow with grain sizes of 100 and 1000 μm. The addition of the same amount of ash caused a greater reduction in albedo for the large grained snow than the smaller grained snow. Hadley and Kirchstetter (2012) showed that artificial snow with three different grain sizes re-sponded differently to additions of black carbon; with a more coarse grained snow showing a greater relative decrease in albedo. Figure S4 in the Supplement of Reay et al. (2012) shows the variation of e-folding depth with increasing black carbon for four different, yet similar, snowpacks at Barrow Alaska; a hard snowpack, soft snowpack, inland snow and snow on sea ice. The e-folding depth of a soft snowpack was slightly more sensitive to the addition of black carbon than the other three snowpacks raising the question if the e-folding depth of different snowpacks would also respond differ-ently to black carbon. Zatko et al. (2013) calculated e-folding depths of Antarctic and Greenland ice sheets considering the effect of increasing mass-ratio of black carbon and grain size independently of each other. Figure 3c of Zatko et al. (2013) shows the decrease in actinic flux with depth in a snowpack is dependent on snow grain size, with a larger decrease observed for smaller grain sizes and Fig. 3b demonstrates the de-creasing e-folding depth with increasing mass-ratio of black carbon. The work of Zatko et al. (2013) is very different to the work presented here which explores the change in albedo and e-folding depth with increasing mass ratio of black carbon as a function of scattering cross-section (i.e. grain size) i.e. quantifying the effect of absorption within the snowpack as a function of scattering cross-section. The work of Reay et al. (2012) was for very similar snowpacks, the work of Warren (1982) was limited to two hypo-thetical types of snow and a few concentrations of light absorbing impurity. The work of Hadley and Kirchstetter (2012) was limited to snow only. A detailed study of exploring the effect of different types of snow and sea ice on the variation of albedo and e-folding depth with black carbon has not previously been attempted. The work presented here expands on the work by Reay et al. (2012) to considering a much larger variety of snowpacks and includes sea ice. To the author's knowledge a *systematic* study of the

response of albedo/*e*-folding depth to black carbon as a function of snow and sea ice type has not been undertaken.

Presented here for the first time are radiative-transfer calculations to quantify how the albedo and *e*-folding depth of three different types of snow (cold polar snow, wind-packed snow and melting snow) and three different types of sea ice (multi-year sea ice, first-year sea ice and melting sea ice) respond to increasing black carbon. Different types of snow and sea ice may be "optically characterised" by a specific scattering-cross section, mass density and asymmetry parameter. Variation in these parameters will result in different albedo and *e*-folding depths and, as will be shown, different responses in these measurements to black carbon.

2   Method

The response of albedo and *e*-folding depth (a measure of light penetration into the snow or sea ice) to increased black carbon for each snow/sea ice was calculated using the radiative-transfer model, TUV-snow, using the DISORT code and described in detail by Lee-Taylor and Madronich (2002). The TUV-snow model is a coupled atmosphere-snow/sea ice radiative-transfer model. The radiative-transfer properties of snow/sea ice are described by an asymmetry factor, g, a wavelength independent scattering cross-section, σ_{scatt}, and wavelength dependant absorption cross-section, σ_{abs}. The total absorption cross-section, σ_{abs}, at a wavelength, λ, is due to absorption by ice, $\sigma_{\text{abs}}^{\text{ice}}$, and absorption by black carbon, σ_{abs}^{+}, (see Eq. 1). For these radiative-transfer calculations described here black carbon is assumed to be the only other absorber present other than ice. However as detailed in the Supplement of Reay et al. (2012) it is possible to convert the results of this paper to other absorbers such as HULIS (HUmic LIke Substances) and mineral dust (e.g. Carmagnola et al. (2013)).

$$\sigma_{\text{abs}}(\lambda) = \sigma_{\text{abs}}^{\text{ice}}(\lambda) + \sigma_{\text{abs}}^{+}(\lambda) \tag{1}$$

Title Page

Abstract | Introduction

Conclusions | References

Tables | Figures

◄ | ►

◄ | ►

Back | Close

Full Screen / Esc

Printer-friendly Version

Interactive Discussion

The asymmetry parameter, g, is taken as a fixed wavelength independent value for sea ice or snow, and the scattering cross-section may be related to the microstructure of snow or sea ice. In the work described here different snowpacks (cold polar snow, windblown snow, melting snow) and different sea ice (multi-year ice, first-year ice and melting ice) are described by different values of the scattering cross-section, described in Sect. 2.1

The TUV-snow model has been previously used for coupled atmosphere-sea ice radiative-transfer calculations (King et al., 2005; Marks and King, 2013), multiple times for coupled atmosphere-snow calculations (Fisher et al., 2005; Beine et al., 2006; France et al., 2007, 2010a, b, 2011, 2012; Reay et al., 2012; Abbatt, 2013; Frey et al., 2013), and validated in laboratory artificial snow experiments by Phillips and Simpson (2005).

2.1 Calculating variation in albedo/e-folding depth response to black carbon for different snow/sea ice types

Upwelling and downwelling irradiances in and above the snow/sea ice to the top of atmosphere were calculated for different snow and sea ice types; cold polar snow, windpacked snow, melting snow, multi-year sea ice, first-year sea ice and melting sea ice. The range of values of the scattering cross-section, density and asymmetry parameter, g, of the snow and sea ice types used in this work are shown in Table 1. The values of mass density and scattering cross-section chosen cover a wide range of possible types of snow and sea ice. Calculations were carried out at densities of 200, 400 and 600 kg m^{-3} for snow and 700, 800, and 900 kg m^{-3} for sea ice. In the results section only the results from the mid-range density of 400 kg m^{-3} for all snow types and 800 kg m^{-3} for all sea ice types is reported, results for other densities are reported in the Supplement. Albedo, $\left(\frac{I_{up}}{I_{down}}\right)$, was calculated as the ratio of upwelling irradiance, I_{up}, to downwelling irradiance, I_{down}, at the surface of the snow or sea ice. The e-folding depth was calculated using Eq. (2), as the distance over which irradiance

Title Page

Abstract | Introduction

Conclusions | References

Tables | Figures

◄ | ►

◄ | ►

Back | Close

Full Screen / Esc

Printer-friendly Version

Interactive Discussion

within the snow or sea ice will reduce to $\frac{1}{e}$ (~37 %) of the original value.

$$\frac{I_z}{I_{z'}} = e^{-\left(\frac{(z-z')}{e}\right)} \tag{2}$$

Where e is e-folding depth, I_z is the downwelling irradiance at depth z, z' is a reference depth, and $I_{z'}$ is the downwelling irradiance, at reference depth, z'.

Albedo and e-folding depth of the different types of snow/sea ice were calculated for mass-ratios of black carbon from 1 to 1024 ng g^{-1} (1, 2, 4, 8, 16, 32, 64, 128, 256, 512 and 1024 ng g^{-1}). For completeness, mixing ratios of black carbon up to 1024 ng g^{-1} have been included as Doherty et al. (2010) reported snow black carbon mass-ratios up to ~500 ng g^{-1}. However, the authors wish to state mass-ratios of black carbon above 100 ng g^{-1} would be considered extremely large and these two larger mass-ratios 512 and 1024 ng g^{-1} have only been included for completeness. The black carbon was assumed to be evenly distributed throughout the snow or sea ice. The absorption spectrum for black carbon in ice was determined by a Mie calculation using the method outlined by Warren and Wiscombe (1980) and used previously by Marks and King (2013) for black carbon in sea ice. The wavelength independent refractive index of spherical black carbon particles is $1.8 \pm 0.5i$, with a diameter of 0.2 µm and density of 1 g m^{-3} (Warren and Wiscombe, 1985, 1980). Comparison of the resulting black carbon absorption spectra with experimentally determined values demonstrates the Mie calculation is realistic (France et al., 2012). The wavelength dependent refractive index of the surrounding ice and the absorption spectrum of ice is taken from Warren and Brandt (2008).

Thicknesses of 10, 1 and 0.5 m were used for snow and sea ice, with extra thicknesses of 0.25 and 0.1 m considered for sea ice and snow respectively. An unrealistic thickness of 10 m was used to calculate albedo and e-folding depths of snow and sea ice which are independent of the underlying ground or seawater. It is useful to understand the effects of black carbon on the albedo and e-folding depth of snow and sea ice independent of snow or sea ice thickness. Such calculations are referred to as

"semi-infinite". So, whilst a thickness of 10 m may be unrealistic in nature it is useful for a general understanding of the important principles/factors effecting the measured optical properties; albedo and *e*-folding depth.

The atmosphere and snow or sea ice are split into levels; Table 2 describes the structure of levels for each snow/sea ice thickness modelled. Calculations of irradiance were undertaken at wavelengths 300–800 nm, using an eight-stream DISORT model with a pseudo-spherical correction (Lee-Taylor and Madronich, 2002). The atmosphere had an ozone column of 300 Dobsons with no atmospheric loading of aerosol and was formed of 66 uneven levels getting progressively thicker upwards from the surface. A wavelength-independent under-snow/sea ice albedo of 0.1 was used and the Earth–Sun distance was set to 1 AU. Diffuse sky conditions were used throughout the work by placing cumulus clouds in the model at a 1 km altitude, with an optical thickness of 16, an asymmetry parameter of 0.85 and a single scattering albedo of 0.9999. Diffuse conditions were used so that albedo of the snow and sea ice could be calculated independent of solar zenith angle. Light penetration depth (*e*-folding depth) through the snow were calculated in the asymptotic zone for semi-infinite snow/sea ice.

3 Results

The results section will report the response of the albedo of snow/sea ice to increasing black carbon as a function of the type of snow and sea ice and secondly the response of *e*-folding depth to the same changes in black carbon mass-ratio and snow or sea ice type. In the results section relative changes in albedo and *e*-folding depth owing to a specific mass-ratio of black carbon for different snow and sea ice types will be examined to enable comparison between different snow and sea ice types. The change in albedo and *e*-folding depth is reported relative to an albedo and *e*-folding depth calculated with a black carbon mass-ratio of 1 ng g^{-1}. The relative change can be expressed mathematically for albedo as, $\frac{A_{BC=1} - A_{BC=x}}{A_{BC=1}}$, and as $\frac{e_{BC=1} - e_{BC=x}}{e_{BC=1}}$, for *e*-folding depth, where

$A_{BC=x}$ is albedo at a black carbon mass-ratio of $x\,\mathrm{ng\,g^{-1}}$ and $e_{BC=x}$ is an e-folding depth at a black carbon mass-ratio of $x\,\mathrm{ng\,g^{-1}}$.

3.1 The response of albedo to increasing mass-ratio of black carbon in semi-infinite snow and sea ice

The albedo of snow is very sensitive to both the mass-ratio of black carbon and snow type, as shown in Fig. 1. Figure 1 shows the calculated albedo of snow as a function of black carbon (increasing absorption cross-section of light absorbing impurity) for the three snowpacks (cold polar snow, windpacked snow and melting snow), at a wavelength of 550 nm and a snow density of $400\,\mathrm{kg\,m^{-3}}$, for a semi-infinite snow. Studying the semi-infinite case (10 m of snow/sea ice) is important in order to able to fairly compare different snow/sea ice types without having any thickness effect. The shaded areas represent the albedo values calculated for the range of scattering cross-sections in Table 1. A melting snowpack shows a considerably larger change in albedo due to additions of black carbon than a windpacked snow and a cold polar snow shows the smallest change. Figure 2a shows the relative change in albedo with increasing mass-ratio of black carbon is different for the three snowpacks. The lines in Fig. 2 represent mid-range relative albedo and e-folding depth values for each snow and sea ice type. The values are calculated using the mid-range albedo and e-folding depth values across the black carbon mass-ratio range examined, for each snow or sea ice type, in Figs. 1, 3, 6 and 7. As will be shown in Sect. 3.3 the change in relative albedo is in contrast to the behaviour of the e-folding depth with increasing mass-ratio of black carbon, as shown in Fig. 2b. The relative change in albedo as a function of increasing black carbon for a melting snow pack is a factor of ∼3.5 larger than the relative change in albedo as a function of increased black carbon for a cold polar snowpack. The equivalent ratio is ∼1.2 for a windpacked snow relative to a cold polar snowpack.

Mathematically the above ratio is expressed in Eq. (3)

$$S = \frac{\left.\frac{A_1 - A_x}{A_1}\right|_{\text{melting}}}{\left.\frac{A_1 - A_x}{A_1}\right|_{\text{cold polar}}} \tag{3}$$

For example, increasing the black carbon in a snowpack from 1 to $50\,\text{ng}\,\text{g}^{-1}$ the relative decrease in cold polar snow albedo is 3 %, for windpacked snow it is 4 % and for melting snow the decrease is 11 %. Note that the ratio in Eq. (3) could be interpreted as how sensitive each snowpack is to increasing black carbon relative to a base case of a cold polar snow. Note the sensitivity is a weak function of mass-ratio of black carbon and the values of 3.5 and 1.2 are useful approximations. Accurate numbers can be determined from Fig. 2a.

The relationships for semi-infinite snow plotted in Figs. 1 and 2a are for a wavelength of light of 550 nm, but is also indicative of the same behaviour for wavelengths of 300–550 nm. Figure S1 in the Supplement shows a more detailed variation of snow albedo as a function of the scattering cross-section range examined for snow (0.5–$25\,\text{m}^2\,\text{kg}^{-1}$) and black carbon mass-ratio (absorption cross-section of light absorbing impurities) at snow densities of 200, 400 and $600\,\text{kg}\,\text{m}^{-3}$ and at wavelengths of 300, 400, 550 and 700 nm rather than the example cases highlighted in Fig. 1. At a wavelength of 700 nm Fig. S1 demonstrates a more pronounced effect. Unsurprisingly at all wavelengths albedo is largest for larger scattering cross-sections (i.e. cold polar snow) (Warren, 1982).

Figure 3 shows the albedo of sea ice as a function of increasing mass-ratio of black carbon (increasing absorption cross-section of snow pack impurity) for the multi-year sea ice, first-year ice, and melting sea ice at a wavelength of 550 nm and a sea ice density of $800\,\text{kg}\,\text{m}^{-3}$. Figure 3, similarly to Fig. 1, shows that the albedo of sea ice is sensitive to the amount of black carbon and type of sea ice. The melting sea ice shows the largest change in albedo due to additions of black carbon and the multi-year sea ice has the smallest change. Figure 2a shows the relative change in albedo with

BC in snow and sea ice

A. A. Marks and
M. D. King

Title Page

Abstract	Introduction
Conclusions	References
Tables	Figures

|◀ | ▶|

◀ | ▶

Back | Close

Full Screen / Esc

Printer-friendly Version

Interactive Discussion

increasing mass-ratio of black carbon is different for the three sea ice. The relative change in albedo as a function of increasing black carbon for a melting ice is a factor of ~2.2 larger than the relative change in albedo as a function of increased black carbon for a multi-year ice (applying Eq. 3). The equivalent ratio is ~1.6 for a first-year ice relative to a multi-year ice. For example for an increase of black carbon from 1 to 50 ng g^{-1} in multi-year sea ice the relative decrease in albedo is 30 %, compared to a decrease of 76 % for melting sea ice.

The albedo of sea ice at wavelengths of 300, 400, 550 and 700 nm as a function of scattering cross-section (0.01–1 m^2 kg^{-1}) and black carbon mass-ratio (absorption cross-section) at sea ice densities of 700, 800 and 900 kg m^{-3} is shown in the Supplement; Fig. S2. Figure S2 is very similar in functional form to Fig. S1 with density having no effect on albedo, as expected, and wavelengths from 300–550 nm showing similar results, with a more pronounced effect at a wavelength of 700 nm. Albedo is obviously largest for the sea ice with largest scattering cross-sections (i.e. multi-year sea ice) for the same mass-ratio of black carbon.

3.2 The response of albedo to increasing black carbon for snow/sea ice with a thickness of 1, 0.5 and 0.25 or 0.1 m

The results presented in Sect. 3.1 are for a 10 m thick snow and sea ice, in reality this is an unrealistic thickness. The thickness of 10 m was chosen so that the snow and sea ice was semi-infinite, thus changes in albedo and e-folding depth were independent of the underlying surface and the albedo response to black carbon of snow or sea ice with small scattering cross-section values could be compared with larger scattering cross-section values. In order to understand the dependence of the results presented in Sect. 3.1 on the thickness of snow or ice the calculations were repeated with more realistic thicknesses of 0.1 m (for snow), 0.25 m (for sea ice) and 0.5 m and 1 m for snow and sea ice. Figures 4 and 5 show the albedo of the three different types of snow/sea ice respectively as a function of black carbon (absorption cross-section of light absorbing impurity) and thickness, at a constant wavelength of 550 nm and a density of

400 kg m^{-3} for the snow and 800 kg m^{-3} for the sea ice. The albedo of the snow, Fig. 4, is much less sensitive to thickness than sea ice (Fig. 5) over the thickness considered. The windpacked snow and cold polar snow show negligible dependance on thickness because they are already semi infinite at the thicknesses considered owing to their large values of scattering cross-section. However, the melting snow is dependant on thickness up to a snow thickness of ~50 cm. Decreased thickness of the melting snow reduces the change in albedo with increasing mass-ratio of black carbon compared to the semi-infinite case. Albedo of all sea ice types, shown in Fig. 5, is dependent on thickness. Reducing the thickness reduces the change in albedo for increasing black carbon. For mass-ratios of black carbon less than 100 ng g^{-1} sea ice albedo increases as the sea–ice thickness increases. The difference in dependence on thickness for snow and sea ice is because snow is semi-infinite at a much smaller thickness than sea ice owing to the larger scattering cross-section of snow relative to sea ice. The results presented in Figs. 4 and 5 are dependant on the albedo of the medium under the snow or sea ice. For the calculations presented here the underlying medium had a wavelength independent albedo of 0.1 to crudely represent soil or seawater (Payne, 1972; Dickinson, 1983).

3.3 The response of e-folding depth to increasing black carbon in semi-infinite snow/sea ice

The variation of light penetration into snow or sea ice (measured by e-folding depth) with black carbon is different to the variation of albedo with black carbon and snow or sea ice type. Although snowpacks and sea ice with smaller scattering cross-sections have longer e-folding depths, the factor by which the e-folding depth decreases as the mass-ratio of black carbon increases is the same for all snow and sea ice. Such behaviour may not be surprising to an expert in radiative transfer but is a useful result to a non-expert studying the climatology, energy balance, photobiology or photochemistry of a snow or sea ice.

Figure 6 shows the *e*-folding depth of snow with increasing mass-ratio of black carbon (increasing absorption cross-section) for the snowpacks at a wavelength of 550 nm and a snow density of 400 kg m^{-3} and Fig. 7 shows variation in sea ice *e*-folding depth with increasing absorption cross-section (black carbon) for the three types of sea ice with a density of 800 kg m^{-3}. Both Figs. 6 and 7 show there is a large change in the *e*-folding depth with increasing mass-ratio of black carbon which is different for snow/sea ice type. However, as shown in Fig. 2b the relative change in *e*-folding depth is effectively the same for different types of snow or sea ice. The relative change in *e*-folding depth as a function of increasing black carbon for a melting snow and a windpacked snow is approximately the same as the relative change in *e*-folding depth as a function of increased black carbon for a cold polar snow (applying Eq. 3). Thus although the absolute change in *e*-folding depth is different for each snow type the relative change is almost the same, in contrast to albedo. The relative decrease in *e*-folding depths with increased mass-ratio of black carbon is again similar for the three sea ice types considered (although a little more different than the three snowpacks considered).

Figures S3 and S4 in the Supplement show snow and sea ice *e*-folding depth at wavelengths of 300, 400, 550 and 700 nm as a function of scattering cross-section (0.01–1 m^2 kg^{-1}) and mass-ratio of black carbon (absorption cross-section of light absorbing impurities) at snow densities of 200, 400 and 600 kg m^{-3} and sea ice densities of 700, 800 and 900 kg m^{-3}. Density obviously affects *e*-folding depth, with a more dense snow or sea ice having slightly shorter *e*-folding depths as explained by Warren (1982). Similarly to Figs. S1 and S2, wavelengths from 300–550 nm show the same behaviour to Figs. 6 and 7 with a more pronounced effect at a wavelength of 700 nm. At all wavelengths *e*-folding depth is shortest for larger scattering cross-sections (i.e. cold polar snow/multi-year sea ice).

BC in snow and sea ice

A. A. Marks and
M. D. King

Title Page

Abstract	Introduction
Conclusions	References
Tables	Figures

◄◄	►►
◄	►
Back	Close

Full Screen / Esc

Printer-friendly Version

Interactive Discussion

3.4 The response of e-folding depth to increasing black carbon in a snow/sea ice with a thickness of 1, 0.5 and 0.25 or 0.1 m

The variation of e-folding depth with mass-ratio of black carbon for different thicknesses of snow and sea ice (0.1, 0.25, 0.5, 1 and 10 m) is shown in Figs. 8 and 9 respectively. Conversely to the variation of albedo with black carbon for different snow and sea ice types the variation of e-folding depth with black carbon for different snow and sea ice types is more sensitive to the thickness of the snow/sea ice. Figure 8 shows the variation of e-folding depth with black carbon for melting snow is most sensitive to thickness, but all snow types are sensitive up to a mass-ratio of black carbon of $\sim 100\,\mathrm{ng\,g}^{-1}$, where the black carbon dominates the absorption of light within the snow or ice (e.g. Reay et al., 2012). The e-folding depth of sea ice, Fig. 9, is more sensitive to thickness than snow, with large variations in e-folding depth observed with different sea ice thicknesses. The most sensitive sea ice is the melting ice. In stark contrast to Figs. 4 and 5, Figs. 8 and 9 demonstrate that as the mass-ratio of black carbon increases then the value of e-folding depth for the different snow/sea ice types trend to a similar value of e-folding depth as the dominant loss of photons in the snow and sea ice becomes absorption by black carbon. Although the absolute values of albedo and e-folding depth may vary with thickness, it is important to consider that the trend for a medium with a larger scattering cross-section to be less responsive to black carbon still exists, an important result for those considering photochemistry and photobiology within the snow/sea ice.

4 Discussion

The calculations presented here show the response of albedo and e-folding depth of snow or sea ice to black carbon is dependent on the snow or sea ice types or scattering cross-section of the snow or sea ice. While it is not surprising that these properties (albedo and light penetration depth) are dependent on scattering cross-section of the

Full Screen / Esc

Printer-friendly Version

Interactive Discussion

snow or sea ice, picking scattering cross-section values to represent realistic snow and sea ice types has enabled quantification of the different response of snow and sea ice types.

The discussion will initially focus on how the choice of snow and sea ice scattering cross-section affects the albedo and *e*-folding depth response to increasing black carbon, then compare the response of snow vs. sea ice. The discussion section will also speculate how climate change may lead to changes in snow/sea ice types commonly observed and the effect this may have on the response to black carbon. Finally some of the parameters used in this work will be critically examined with a view to describing the robustness of the work presented here.

4.1 The role of scattering cross-section in determining snow/sea ice response to black carbon

Figs. 1, 2a and 3 (and Supplement S1 and S2) show that a snow and sea ice with a large scattering cross section, e.g. cold polar snow and multi-year ice show a smaller change in albedo owing to additions of black carbon than the snow or sea ice with a smaller scattering cross-section. Warren (1982) and Aoki et al. (2003) stated that albedo of a snowpack decreases as grain size of that snowpack increases, with Kokhanovsky and Zege (2004) demonstrating that scattering cross-sections of snow may be inversely proportional to grain size of snow. Warren (1982) explain this phenomenon as photons are scattered at air–ice interfaces and absorbed passing through ice. In a snow/sea ice with a larger scattering cross-section (smaller grain size) a photon propagates less far through a snowpack before it is scattered out, so it has less opportunity to be absorbed by any black carbon in the sea ice/snow before it exits the snow pack, thus the albedo is higher. Although the work here demonstrates the known result that an increase in scattering cross-section (typically smaller grain size for snow) results in smaller changes to albedo owing to an increase in black carbon than for a smaller scattering cross-section (typically a larger grain size), the authors believe this is the first time it has been quantified for three characteristic snowpacks

and sea ice (and calculated in detail in the Supplement). The factor by which e-folding depths decrease with increasing mass-ratio of black carbon is almost independent of the type of snow or sea ice.

4.2 The response of snow vs. sea ice

Calculations of the albedo of both snow and sea ice to increased black carbon enables comparison between the response of the two mediums. The albedo of sea ice is far more responsive to additions of black carbon than the albedo of snow, as briefly suggested by Bond et al. (2013). For example, according to Figs. 1 and 3, for a first-year sea ice and a windpacked snow, there is a relative decrease in albedo of 57 % and 4 % respectively, with a black carbon increase from 1 to 50 $ng\,g^{-1}$. The different albedo response of snow and sea ice to increased black carbon is clearly shown in Fig. 2a.

As noted in Sect. 3.3 the e-folding depth is sensitive to the mass-ratio of black carbon and the type of snow or sea ice; but the relative change in e-folding depth is insensitive to the type of snow or sea ice. For example, Figs. 6 and 7 show that for a windpacked snow compared to a first-year sea ice a relative change in e-folding depth to 22 % and 20 % of the original e-folding depth respectively occurs, for a black carbon increase from 1 to 50 $ng\,g^{-1}$. Workers studying the photobiology and photochemistry of snow and sea ice and need to know the light penetration can use Fig. 2 as a rough rule to calculate how a change in black carbon may change the light penetration depth of solar radiation.

4.3 "Semi-infinite snow/sea ice"

For some of the calculations presented here a thickness of 10 m is used to ensure semi-infinite snow/sea ice is achieved and thus the snow/sea ice is independent of the underlying medium to allow comparison. France et al. (2011) report that a snowpack is semi-infinite after 3–4 e-folding depths. For the majority of snowpacks examined here the snow would be semi-infinite at about 1 m.

BC in snow and sea ice

A. A. Marks and
M. D. King

Title Page

Abstract | Introduction

Conclusions | References

Tables | Figures

◄ | ►

Back | Close

Full Screen / Esc

Printer-friendly Version

Interactive Discussion

However, for snow with a very small scattering cross-section ($< 1\,\mathrm{m^2\,kg^{-1}}$) or small black carbon mass-ratio ($< 5\,\mathrm{ng\,g^{-1}}$) the thickness at which semi-infinite occurs increases to over 2 m (but less than 10 m). In the case of sea ice semi-infinite would occur before a thickness of 5 m, increasing to 10 m for the small densities, scattering cross-section $< 0.025\,\mathrm{m^2\,kg^{-1}}$) or black carbon mass-ratios ($< 5\,\mathrm{ng\,g^{-1}}$). Note that for all optical properties in the work presented here and in the Supplement the 10 m thickness is sufficient for the semi-infinite approximation.

4.4 Wider implications of the work

The 2007 IPCC report (Solomon et al., 2007) describes potential changes that may occur to snow cover and sea ice as a result of climate change. The Arctic summer sea ice extent has decreased ($-7.4\,\%$ a decade) which has lead to a decrease in multi-year sea ice in favour of first-year sea ice (Solomon et al., 2007). As shown here, first-year ice is more responsive to black carbon additions than the multi-year ice, which could potentially exacerbate sea ice melting. Furthermore as first-year ice transforms into melting ice it becomes even more responsive to black carbon additions, further exacerbating sea ice melting. A similar scenario can be hypothesised for snow.

4.5 An assessment of uncertainty

The calculations presented here show the effect that changes in scattering cross-section of snow and sea ice have on the e-folding depth and albedo response to increased mass-ratio of black carbon. The calculations assumed the asymmetry parameter, g, and the optical properties of black carbon were unchanged with snow and sea ice type. The effect of changing these properties is considered to be secondary to the effect of changing black carbon mass-ratio, scattering cross-section and density (Reay et al., 2012).

The value of the asymmetry parameter, g, was 0.89 for snow (Warren and Wiscombe, 1980) and 0.98 for sea ice (Mobley et al., 1998). Warren and Wiscombe (1980)

Mie calculations for wavelengths less than 1000 nm show g is practically invariant with wavelength ($g \approx 0.89$) for snow. Mobley et al. (1998) calculated asymmetry parameters for sea ice from Mie calculations that gave a range from 0.96 to 0.99, based on air bubble content, with a smaller bubble content giving a higher value of g, the most likely value is 0.98. The values of g used here are therefore commonly reported as the most likely values for snow/sea ice at the wavelengths investigated. Small changes in g (± 0.005) have very little effect on the albedo and e-folding depths reported, as shown by France et al. (2012) for snow and Marks and King (2013) for sea ice.

The optical properties of the particulate black carbon used for calculations presented here (refractive index, size and density) are taken as a standard for black carbon and are based on calculations by Warren and Wiscombe (1980, 1985). Certain limitations were suggested by Bohren (1986) who reviewed uncertainties in the black carbon constants, a discussion of the effects of these uncertainties can be found in Marks and King (2013). France et al. (2012) use the same properties of black carbon as presented here and show a good correlation between calculated black carbon absorption cross-section and the experimental black carbon absorption cross-section as reviewed by Bond and Bergstrom (2006).

5 Conclusions

The response of albedo of snow/sea ice to increased mass-ratios of black carbon is dependent on the type of snow and sea ice. A snow or sea ice with a large scattering cross-section, e.g. a cold polar snow or a multi-year sea ice is less responsive to black carbon than a melting snow or sea ice. The change in albedo owing to increasing black carbon is less in snow than sea ice. For an increase of black carbon from 1 to 50 ng g^{-1} a relative change in albedo of 76 % occurs for melting sea ice compared to 30 % for multi-year ice, 11 % for melting snow and 3 % for cold polar snow. In the case of e-folding depth the snow and sea ice type has very little affect on the relative response due to increased black carbon. Current climate change is leading to a decrease in

multi-year sea ice and an increase in first-year/melting sea ice, which would be more responsive to black carbon, potentially exacerbating sea ice melting rates.

Supplementary material related to this article is available online at http://www.the-cryosphere-discuss.net/8/1023/2014/tcd-8-1023-2014-supplement.pdf.

References

Abbatt, J.: Atmospheric chemistry: arctic snowpack bromine release, Nat. Geosci., 6, 331–332, 2013. 1028

Aoki, T., Hachikubo, A., and Hori, M.: Effects of snow physical parameters on shortwave broad-band albedos, J. Geophys. Res., 108, 4916, doi:10.1029/2003JD003506, 2003. 1037

Beine, H. J., Amoroso, A., Dominé, F., King, M. D., Nardino, M., Ianniello, A., and France, J. L.: Surprisingly small HONO emissions from snow surfaces at Browning Pass, Antarctica, Atmos. Chem. Phys., 6, 2569–2580, doi:10.5194/acp-6-2569-2006, 2006. 1028

Bohren, C.: Applicability of effective-medium theories to problems of scattering and absorption by nonhomogeneous atmospheric particles, J. Atmos. Sci., 43, 468–475, 1986. 1040

Bond, T. and Bergstrom, R.: Light absorption by carbonaceous particles: an investigative review, Aerosol Sci. Tech., 40, 27–67, 2006. 1040

Bond, T., Doherty, S., Fahey, D., Forster, P., Berntsen, T., DeAngelo, B., Flanner, M., Ghan, S., Kärcher, B., and Koch, D.: Bounding the role of black carbon in the climate system: a scientific assessment, J. Geophys. Res.-Atmos., 118, 5380–5552, 2013. 1024, 1025

Carmagnola, C. M., Domine, F., Dumont, M., Wright, P., Strellis, B., Bergin, M., Dibb, J., Picard, G., Libois, Q., Arnaud, L., and Morin, S.: Snow spectral albedo at Summit, Greenland: measurements and numerical simulations based on physical and chemical properties of the snowpack, The Cryosphere, 7, 1139–1160, doi:10.5194/tc-7-1139-2013, 2013. 1027

Chýlek, P., Ramaswamy, V., and Srivastava, V.: Albedo of soot-contaminated snow, J. Geophys. Res., 88, 10837–10843, 1983. 1024

Clarke, A. and Noone, K.: Soot in the Arctic snowpack: a cause for perturbations in radiative transfer, Atmos. Environ., 19, 2045–2053, 1985. 1024

5 Dickinson, R.: Land surface processes and climate–surface albedos and energy balance, in: Advances in Geophysics, vol. 25, Academic Press, New York, USA, 1983. 1034

Doherty, S. J., Warren, S. G., Grenfell, T. C., Clarke, A. D., and Brandt, R. E.: Light-absorbing impurities in Arctic snow, Atmos. Chem. Phys., 10, 11647–11680, doi:10.5194/acp-10-11647-2010, 2010. 1025, 1029

10 Fisher, F., King, M., and Lee-Taylor, J.: Extinction of UV-visible radiation in wet midlatitude (maritime) snow: implications for increased NO_x emission, J. Geophys. Res., 110, D21301, doi:10.1029/2005JD005963, 2005. 1028, 1046

Flanner, M., Zender, C., Randerson, J., and Rasch, P.: Present-day climate forcing and response from black carbon in snow, J. Geophys. Res., 112, D11202, doi:10.1029/2006JD008003, 2007. 1025

15 France, J.: Chemical Oxidation in Snowpacks, Ph.D. thesis, Royal Holloway, University of London, 2008. 1046

France, J. L., King, M., and Lee-Taylor, J.: Hydroxyl (OH) radical production rates in snowpacks from photolysis of hydrogen peroxide (H_2O_2) and nitrate (NO_3^-), Atmos. Environ., 41, 5502–5509, 2007. 1028

20 France, J. L., King, M., and Lee-Taylor, J.: The importance of considering depth-resolved photochemistry in snow: a radiative-transfer study of NO_2 and OH production in Ny-Alesund (Svalbard), J. Glaciol., 56, 655–663, 2010a. 1028

France, J. L., King, M., and MacArthur, A.: A photohabitable zone in the martian snowpack? 25 A laboratory and radiative-transfer study of dusty water–ice snow, Icarus, 207, 133–139, 2010b. 1028

France, J. L., King, M. D., Frey, M. M., Erbland, J., Picard, G., Preunkert, S., MacArthur, A., and Savarino, J.: Snow optical properties at Dome C (Concordia), Antarctica; implications for snow emissions and snow chemistry of reactive nitrogen, Atmos. Chem. Phys., 11, 9787–30 9801, doi:10.5194/acp-11-9787-2011, 2011. 1028, 1038, 1046

France, J. L., Reay, H., King, M., Voison, D., Jacobi, H., Domine, F., Beine, H., Anastasio, C., MacArthur, A., and Lee-Taylor, J.: Hydroxyl radical and NO_x producion rates, black carbon concentrations and light-absorbing impurities in the snow from field measurements of light

penetration and nadir reflectivity of on-shore and off-shore coastal Alaskan snow, J. Geophys. Res., 117, D00R12, doi:10.1029/2011JD016639, 2012. 1025, 1028, 1029, 1040

Frey, M. M., Brough, N., France, J. L., Anderson, P. S., Traulle, O., King, M. D., Jones, A. E., Wolff, E. W., and Savarino, J.: The diurnal variability of atmospheric nitrogen oxides (NO and NO_2) above the Antarctic Plateau driven by atmospheric stability and snow emissions, Atmos. Chem. Phys., 13, 3045–3062, doi:10.5194/acp-13-3045-2013, 2013. 1028

Gerland, S., Winther, J., Ørbæk, J., Liston, G., Øritsland, N., Blanco, A., and Ivanov, B.: Physical and optical properties of snow covering Arctic tundra on Svalbard, Hydrol. Process., 13, 2331–2343, 1999. 1046

Goldenson, N., Doherty, S. J., Bitz, C. M., Holland, M. M., Light, B., and Conley, A. J.: Arctic climate response to forcing from light-absorbing particles in snow and sea ice in CESM, Atmos. Chem. Phys., 12, 7903–7920, doi:10.5194/acp-12-7903-2012, 2012. 1025

Grenfell, T. and Maykut, G.: The optical properties of ice and snow in the Arctic Basin, J. Glaciol., 18, 445–463, 1977. 1046

Grenfell, T., Light, B., and Sturm, M.: Spatial distribution and radiative effects of soot in the snow and sea ice during the SHEBA experiment: the surface heat budget of arctic ocen (SHEBA), J. Geophys. Res., 107, 8032, doi:10.1029/2000JC000414, 2002. 1024

Hadley, O. and Kirchstetter, T.: Black-carbon reduction of snow albedo, Nature Reports Clim. Change, 2, 437–440, 2012. 1025, 1026

Hansen, J. and Nazarenko, L.: Soot climate forcing via snow and ice albedos, P. Natl. Acad. Sci. USA, 101, 423–428, 2004. 1024

Highwood, E. and Kinnersley, R.: When smoke gets in our eyes: the multiple impacts of atmospheric black carbon on climate, air quality and health, Environ. Int., 32, 560–566, 2006. 1024

Holland, M., Bailey, D., Breigleb, B., Light, B., and Hunke, E.: Improved sea ice short wave radiation physics in CCSM4: the impact of melt ponds and aerosols on Arctic sea ice, J. Climate, 25, 1413–1430, 2012. 1025

Jacobson, M.: Strong radiative heating due to the mixing state of black carbon in atmospheric aerosols, Nature, 409, 695–697, 2001. 1024

Jacobson, M.: Climate response of fossil fuel and biofuel soot, accounting for soot's feedback to snow and sea ice albedo and emissivity, J. Geophys. Res., 109, D21201, doi:10.1029/2004JD004945, 2004. 1025

BC in snow and sea ice

A. A. Marks and M. D. King

Title Page

Abstract	Introduction
Conclusions	References
Tables	Figures

|◄ | ►|

◄ | ►

Back | Close

Full Screen / Esc

Printer-friendly Version

Interactive Discussion

King, M., France, J., Fisher, F., and Beine, H.: Measurement and modelling of UV radiation penetration and photolysis rates of nitrate and hydrogen peroxide in Antarctic sea ice: an estimate of the production rate of hydroxyl radicals in first-year sea ice, J. Photoch. Photobio. A, 176, 39–49, 2005. 1028, 1046

5 Kokhanovsky, A. and Zege, E.: Scattering optics of snow, Appl. Optics, 43, 1589–1602, 2004. 1037

Ledley, T. and Thompson, S.: Potential effect of nuclear war smokefall on sea ice, Climatic Change, 8, 155–171, 1986. 1024

Lee-Taylor, J. and Madronich, S.: Calculation of actinic fluxes with a coupled atmosphere-snow
10 radiative transfer model, J. Geophys. Res., 107, 4796, doi:10.1029/2002JD002084, 2002. 1027, 1030

Light, B., Eicken, H., Maykut, G., and Grenfell, T.: The effect of included particulates on the spectral albedo of sea ice, J. Geophys. Res., 103, 27739–27752, 1998. 1024

Marks, A. A. and King, M. D.: The effects of additional black carbon on the albedo of Arc-
15 tic sea ice: variation with sea ice type and snow cover, The Cryosphere, 7, 1193–1204, doi:10.5194/tc-7-1193-2013, 2013. 1028, 1029, 1040, 1046

Mitchell, J.: Visual range in the polar regions with particular reference to the Alaskan Arctic, J. Atmos. Terr. Phys., 195, 195–211, 1957. 1024

Mobley, C., Cota, G., Grenfell, T., Maffione, R., Pegau, W., and Perovich, D.: Modeling light
20 propagation in sea ice, IEEE T. Geosci. Remote, 36, 1743–1749, 1998. 1039, 1040

Painter, T., Bryant, A., and Skiles, S.: Radiative forcing by light absorbing impurities in snow from MODIS surface reflectance data, Geophys. Res. Lett., 39, 17, doi:10.1029/2012GL052457, 2012. 1025

Payne, R.: Albedo of the sea surface, J. Atmos. Sci., 29, 959–970, 1972. 1034

25 Perovich, D.: Theoretical estimates of light reflection and transmission by spatially complex and temporally varying sea ice covers, J. Geophys. Res., 95, 9557–9567, 1990. 1046

Perovich, D.: The Optical Properties of Sea Ice, US Army Corps of Engineers: Cold Regions Research and Engineering Laboratory, US Army Cold Regions Research and Engineering Laboratory,Virginia, USA, 96, 1996. 1025, 1046

30 Phillips, G. and Simpson, W.: Verification of snowpack radiation transfer models using actinom-etry, J. Geophys. Res., 110, D08306, doi:10.1029/2004JD005552, 2005. 1028

Ramanathan, V. and Carmichael, G.: Global and regional climate changes due to black carbon, Nat. Geosci., 1, 221–227, 2008. 1024

Title Page

Abstract | Introduction

Conclusions | References

Tables | Figures

|◄ | ►|

◄ | ►

Back | Close

Full Screen / Esc

Printer-friendly Version

Interactive Discussion

Reay, H., France, J., and King, M.: Decreased albedo, efolding depth and photolytic OH radical and NO_2 production with increasing black carbon content in Arctic snow., J. Geophys. Res., 117, D00R20, doi:10.1029/2011JD016630, 2012. 1025, 1026, 1027, 1028, 1036, 1039

Simpson, W., King, M., Beine, H., Honrath, R., and Zhou, X.: Radiation-transfer modeling of snow-pack photochemical processes during ALERT 2000, Atmos. Environ., 36, 2663–2670, 2002. 1046

Solomon, S., Qin, D., Manning, M., Chen, Z., Marquis, M., Averyt, K., Tignor, M., and Miller, H.: IPCC, 2007: Climate Change 2007: The Physical Science Basis. Contribution of Working Group I to the Fourth Assessment, Report of the Intergovernmental Panel on Climate Change, Cambridge University Press, Cambridge, UK, New York, NY, USA, 2007. 1025, 1039

Timco, G. and Frederking, R.: A review of sea ice density, Cold Reg. Sci. Technol., 24, 1–6, 1996. 1046

Warren, S.: Optical properties of snow, Rev. Geophys. Space GE, 20, 67–89, 1982. 1025, 1026, 1032, 1035, 1037

Warren, S.: Optical constants of ice from the ultraviolet to the microwave, Appl. Optics, 23, 1206–1225, 1984. 1024

Warren, S. and Brandt, R.: Optical constants of ice from the ultraviolet to the microwave: a revised compilation, J. Geophys. Res., 113, 1206–1225, 2008. 1029

Warren, S. and Clarke, A.: Soot in the atmosphere and snow surface of Antarctica, J. Geophys. Res., 95, 1811–1816, 1990. 1024

Warren, S. and Wiscombe, W.: A model for the spectral albedo of snow. II: Snow containing atmospheric aerosols, J. Atmos. Sci., 37, 2734–2745, 1980. 1025, 1029, 1039, 1040

Warren, S. and Wiscombe, W.: Dirty snow after nuclear war, Nature, 313, 467–470, 1985. 1024, 1029, 1040

Yasunari, T., Koster, R., Lau, K., Aoki, T., Sud, Y., Yamazaki, T., Motoyoshi, H., and Kodama, Y.: Influence of dust and black carbon on the snow albedo in the NASA Goddard Earth Observing System version 5 land surface model, J. Geophys. Res., 116, D02210, doi:10.1029/2010JD014861, 2011. 1025

Zatko, M. C., Grenfell, T. C., Alexander, B., Doherty, S. J., Thomas, J. L., and Yang, X.: The influence of snow grain size and impurities on the vertical profiles of actinic flux and associated NO_x emissions on the Antarctic and Greenland ice sheets, Atmos. Chem. Phys., 13, 3547–3567, doi:10.5194/acp-13-3547-2013, 2013. 1025, 1026

Discussion Paper | Discussion Paper | Discussion Paper | Discussion Paper | Discussion Paper

A. A. Marks and
M. D. King

Title Page

Abstract | Introduction

Conclusions | References

Tables | Figures

|◀ | ▶|

◀ | ▶

Back | Close

Full Screen / Esc

Printer-friendly Version

Interactive Discussion

Table 1. Properties of snow and sea ice types studied. Optical and physical properties are based on work by Grenfell and Maykut (1977); Perovich (1990); Timco and Frederking (1996); Perovich (1996); Gerland et al. (1999); Fisher et al. (2005); King et al. (2005); France (2008); France et al. (2011); Marks and King (2013); Simpson et al. (2002).

Snow/sea ice type	Scattering cross-section $(m^2\,kg^{-1})$	Density $(kg\,m^{-3})$	Asymmetry parameter (g)
Cold polar snow	15–25	200–600	0.89
Windpacked snow	5–10	200–600	0.89
Melting snow	0.5–2	200–600	0.89
Frozen multi-year sea ice	0.5–1	700–950	0.98
Frozen first-year sea ice	0.1–0.2	700–950	0.98
Melting sea ice	0.01–0.05	700–950	0.98

Table 2. Level structure utilised for layers of snow/sea ice with different thicknesses and for the atmosphere.

Snow/sea ice thickness (m)	Number of levels	Level structure
0.1	25	1 mm increments from 0–1 cm 1 cm increments from 1–9 cm 1 mm increments from 9.5 to 10 cm
0.25	40	1 mm increments from 0–1 cm 1 cm increments from 1–24 cm 1 mm increments from 24.5 to 25 cm
0.5	38	1 mm increments from 0–1 cm 1 cm increments from 1–10 cm 10 cm increments from 10 to 40 cm 1 cm increments from 40–49 1 mm increments from 49–50 cm
1	30	1 cm increments from 1–10 cm 10 cm increments from 10–90 cm 1 cm increments from 95 to 99 cm 1 mm increments from 99–100 cm
10	47	1 cm increments from 1–10 cm 10 cm increments from 10–90 cm 1 m increments from 100 to 900 cm 10 cm increments from 900–990 cm 1 mm increments from 990–1000 cm
Atmosphere (90 km thick)	80	10 m increments from 10–100 m 100 m increments from from 100–1000 m 1 km increments from 1–10 km 2 km increments from 10–90 km
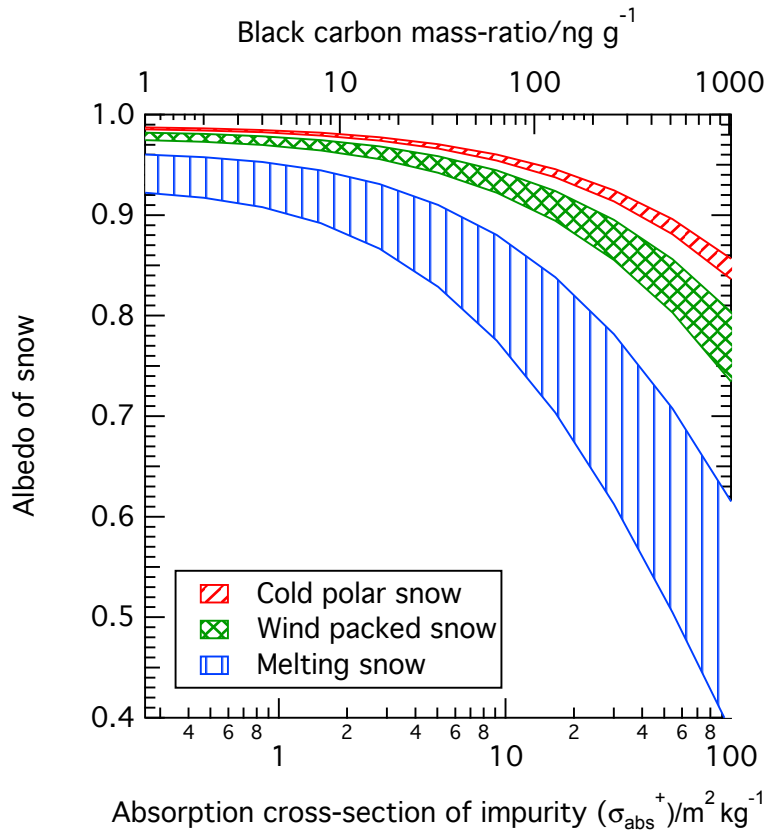
Fig. 1. Albedo with black carbon mass-ratio (top abcissa axis) and increasing absorption cross-section of light absorbing impurities (bottom abcissa axis) for different snow types; cold polar snow (red), windpacked snow (green) and melting snow (blue). The shaded areas show the range of albedo possible for a certain snow type, as described in Table 1. Snow density is $400\,\mathrm{kg\,m^{-3}}$ for all snow types.

Title Page

Abstract | Introduction

Conclusions | References

Tables | Figures

|◄ | ►|

◄ | ►

Back | Close

Full Screen / Esc

Printer-friendly Version

Interactive Discussion
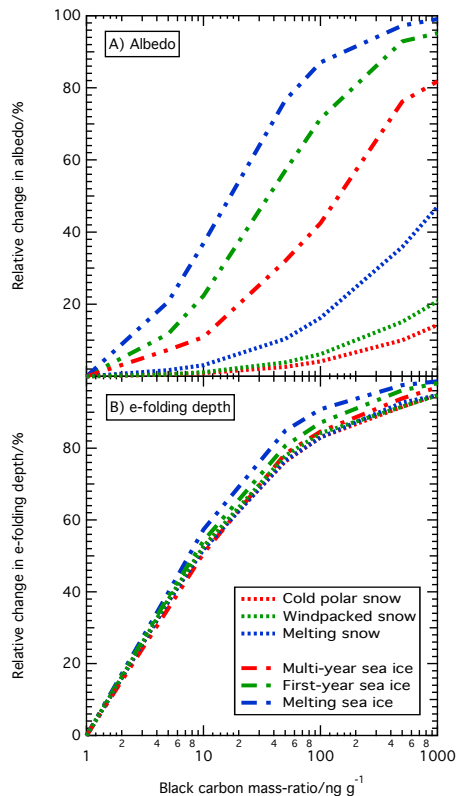
Fig. 2. Relative change in albedo and *e*-folding depth. Each line shows a typical albedo or *e*-folding depth for a particular snow or sea ice type with increasing mass-ratio of black carbon relative to a mass-ratio of black carbon of $1\,\mathrm{ng\,g^{-1}}$. The albedo and *e*-folding depth values are taken as the mid-value for each snow and sea ice from Figs. 1, 3, 6 and 7, across the mass-ratio of black carbon examined. Snow density is $400\,\mathrm{kg\,m^{-3}}$ for all snow types and sea ice density is $800\,\mathrm{kg\,m^{-3}}$ for all sea ice types.
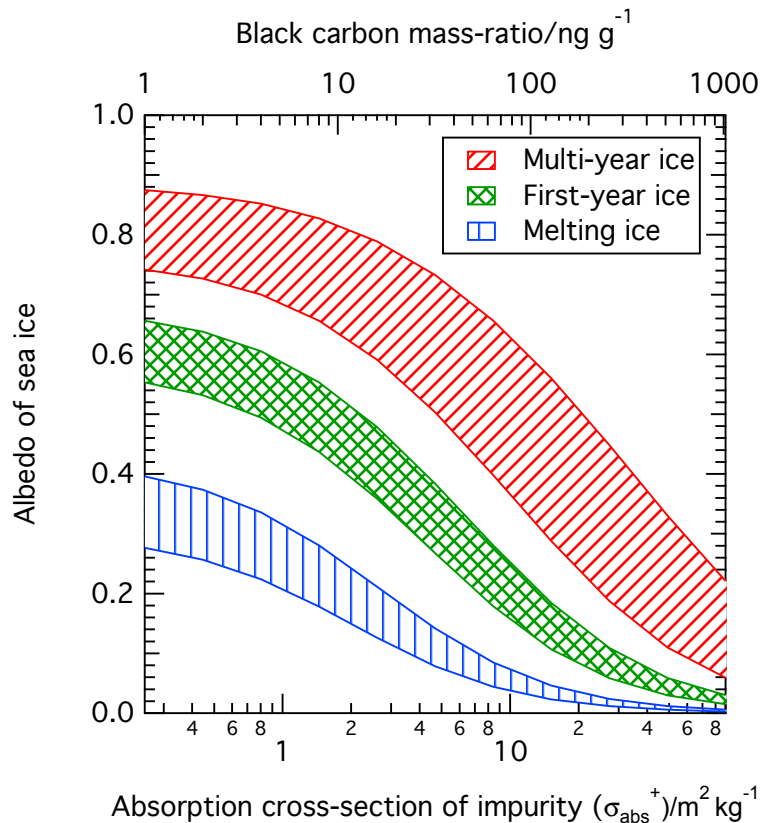
Fig. 3. Albedo with increasing absorption cross-section of light absorbing impurities (bottom abcissa axis) and black carbon mass-ratio (top abcissa axis) for different sea ice types; multi-year ice (red), first-year ice (green) and melting ice (blue). The shaded areas show the range of albedo possible for certain sea ice type, as described in Table 1. Sea ice density is $800 \, \text{kg} \, \text{m}^{-3}$ for all sea ice types.

Title Page

Abstract | Introduction

Conclusions | References

Tables | Figures

|◄ | ►|

◄ | ►

Back | Close

Full Screen / Esc

Printer-friendly Version

Interactive Discussion
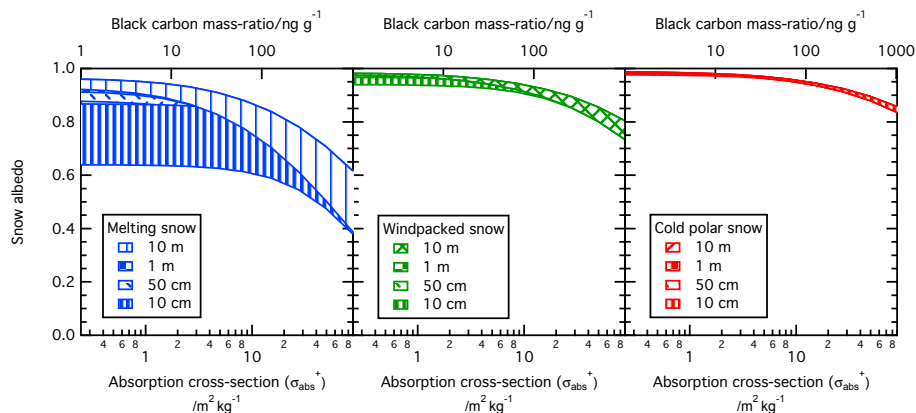
Fig. 4. Albedo of three snow types (cold polar snow, windpacked snow and melting snow) with increasing black carbon mass-ratio (absorption cross-section of light absorbing impurities) for snow thicknesses of 0.1, 0.5, 1 and 10 m. The shaded areas show the range of albedo possible for a certain thickness and snow type, as described in Table 1. A thinner, melting, snowpack is less sensitive to the mass loading of black carbon relative to a semi-infinite thickness. Snow density is $400\,\text{kg}\,\text{m}^{-3}$ for all snow types.

Title Page

Abstract | Introduction

Conclusions | References

Tables | Figures

Back | Close

Full Screen / Esc

Printer-friendly Version

Interactive Discussion
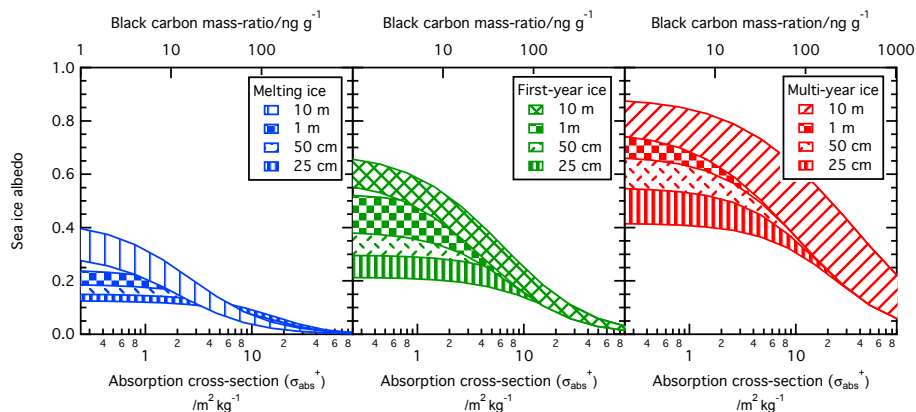
Fig. 5. Albedo of three types of sea ice (multi-year ice, first-year ice and melting ice) with increasing black carbon mass-ratio (absorption cross-section of light absorbing impurities) for sea ice thicknesses of 0.25, 0.5, 1 and 10 m. The shaded areas show the range of albedo possible for certain thickness and sea ice type, as described in Table 1. A thinner sea ice is less sensitive to changes in the mass-ratio of black carbon relative to a semi-infinite thickness. Sea ice density is 800 kg m^{-3} for all sea ice types.

Discussion Paper | Discussion Paper | Discussion Paper | Discussion Paper |

TCD

8, 1023–1056, 2014

BC in snow and sea ice

A. A. Marks and M. D. King

Title Page

Abstract | Introduction

Conclusions | References

Tables | Figures

◄ | ►

◄ | ►

Back | Close

Full Screen / Esc

Printer-friendly Version

Interactive Discussion
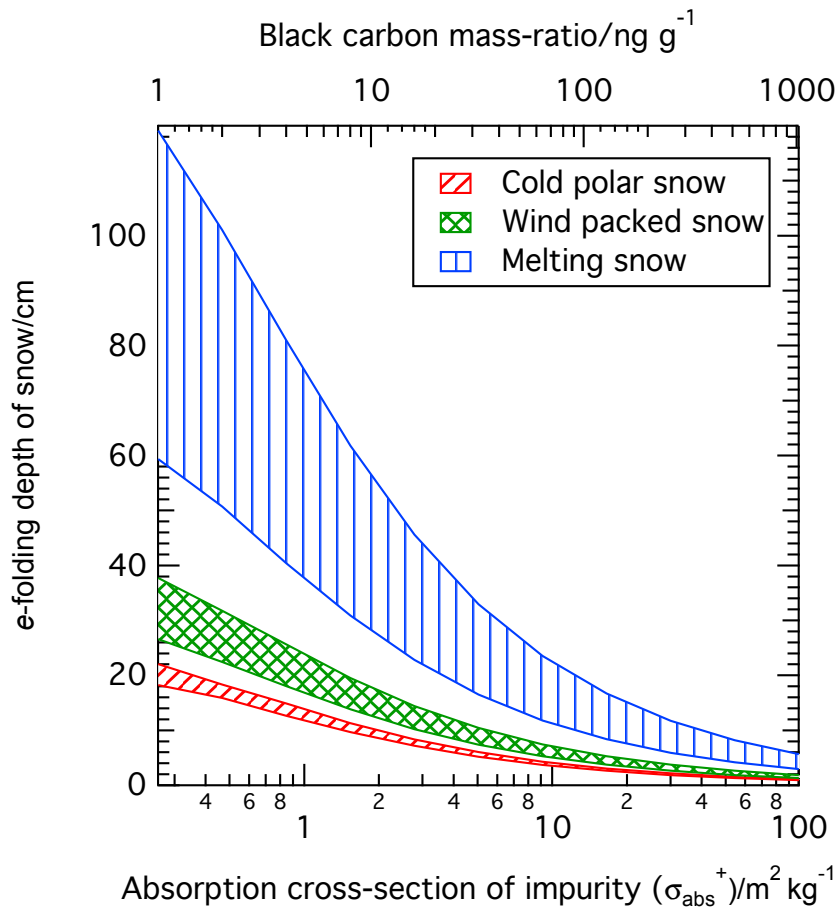
Fig. 6. The *e*-folding depth with increasing black carbon mass-ratio (absorption cross-section of light absorbing impurities) for different snow types; cold polar snow, windpacked snow and melting snow. Snow density is $400\,kg\,m^{-3}$ for all snow types.
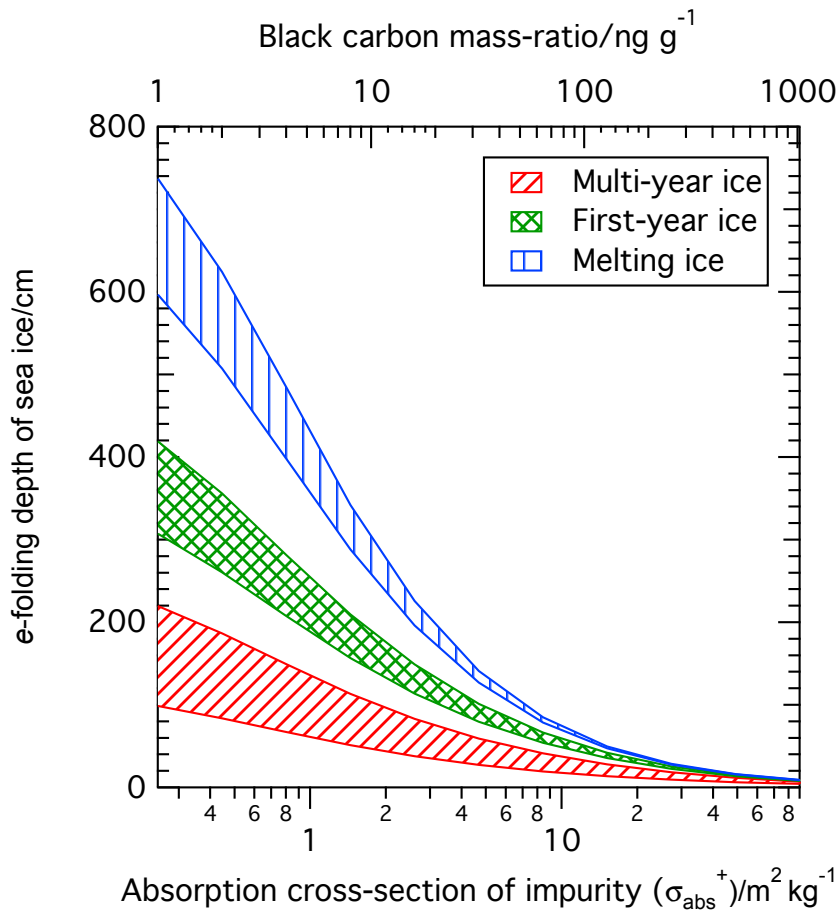
Fig. 7. The *e*-folding depth with increasing black carbon mass-ratio (absorption cross-section of light absorbing impurities) for different sea ice types; multi-year ice, first-year ice and and melting ice. Sea ice density is $800\,\mathrm{kg\,m^{-3}}$ for all sea ice types.
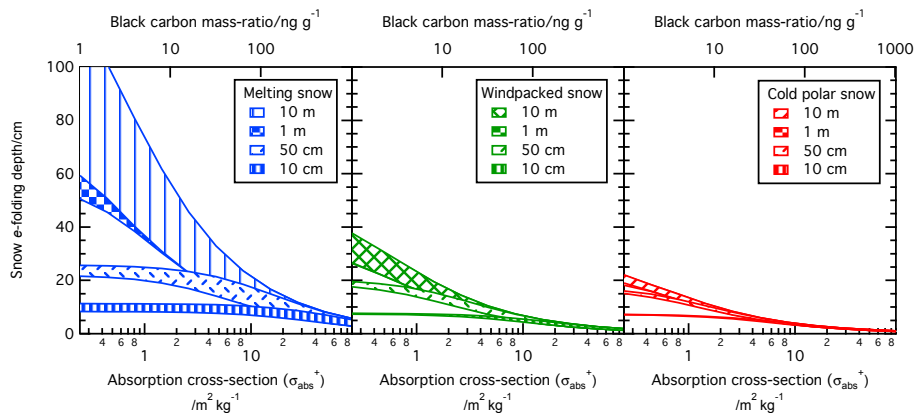
Fig. 8. The *e*-folding depth of snow with increasing black carbon mass-ratio (absorption cross-section of light absorbing impurities) for snow thicknesses of 0.1, 0.5, 1 and 10 m. Snow density is $400\,\mathrm{kg\,m^{-3}}$ for all snow types.
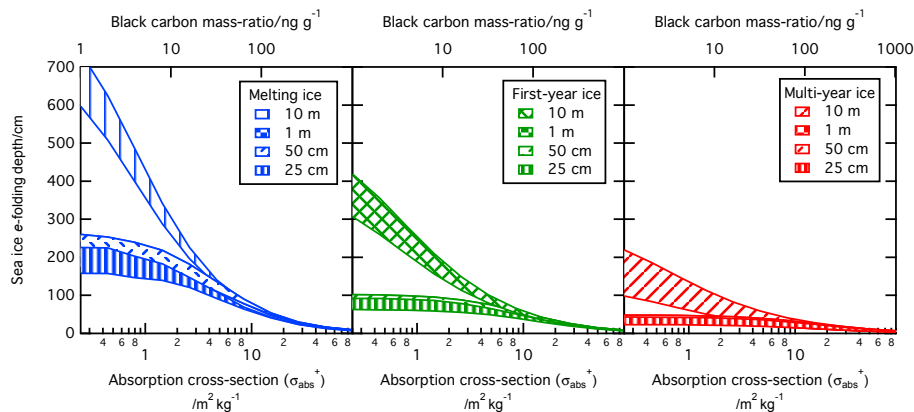
Fig. 9. Sea ice *e*-folding depth with increasing black carbon mass-ratio (absorption cross-section of light absorbing impurities) for sea ice thicknesses of 0.25, 0.5, 1 and 10 m. Sea ice density is 800 kg m^{-3} for all sea ice types.